# Exploiting dissipative reactions to perform in-beam $\gamma$ -ray spectroscopy of the neutron-deficient isotopes $^{38,39}$ Ca

A. Gade , 1,2 D. Weisshaar , 1 B. A. Brown , 1,2 D. Bazin , 1,2 K. W. Brown, 1,3 R. J. Charity , 4 P. Farris, 1,2 A. M. Hill, 1,2 J. Li, 1 B. Longfellow, 1,2,\* D. Rhodes, 1,2,† W. Reviol , 5 and J. A. Tostevin 6 1 Facility for Rare Isotope Beams, Michigan State University, East Lansing, Michigan 48824, USA 2 Department of Physics and Astronomy, Michigan State University, East Lansing, Michigan 48824, USA 3 Department of Chemistry, Michigan State University, East Lansing, Michigan 48824, USA 4 Department of Chemistry, Washington University, St. Louis, Missouri 63130, USA 5 Physics Division, Argonne National Laboratory, Argonne, Illinois 60439, USA 6 Department of Physics, Faculty of Engineering and Physical Sciences, University of Surrey, Guildford, Surrey GU2 7XH, United Kingdom

(Received 27 August 2022; accepted 14 November 2022; published 7 December 2022)

The neutron-deficient Ca isotopes continue to attract attention due to their importance for testing isospin symmetry and their relevance in capture reactions of interest for nova nucleosynthesis and the shape of light curves in Type I x-ray bursts. To date, spectroscopic information on  $^{38,39}$ Ca is largely limited to data on lower-spin excited states. Here, we report in-beam  $\gamma$ -ray spectroscopy of complementary higher-spin, complex-structure states in  $^{39}$ Ca populated in fast-beam-induced, momentum-dissipative processes leading to neutron pickup onto excited configurations of the projectile,  $^{9}$ Be( $^{38}$ Ca\*,  $^{39}$ Ca + $\gamma$ )X. Such a dissipative reaction was recently characterized for the case of inelastic scattering of  $^{38}$ Ca off  $^{9}$ Be( $^{38}$ Ca,  $^{38}$ Ca,  $^{38}$ Ca + $\gamma$ )X. Additional data and discussion on the nuclear structure of  $^{38}$ Ca is also presented. An explanation for the more-complex-structure states, populated with small cross sections in one-nucleon knockout reactions, and observed in the tails of their longitudinal momentum distributions, is also offered.

DOI: 10.1103/PhysRevC.106.064303

#### I. INTRODUCTION

The study of the structure of rare isotopes is fueled by an increasing body of complementary experimental data that reach further and further into the territory of high isospin. Here, changes in the nuclear structure challenge nuclear theory in the quest for a predictive model of nuclei. Often, direct reactions or inelastic scattering processes are used in experimental studies that select single-particle or collective degrees of freedom, predominantly, providing information on lowlying states. Complex-configuration, higher-spin states near the yrast line that may be part of collective, band-like structures have traditionally been accessed with fusion-evaporation reactions on the neutron-deficient side of the nuclear chart when suitable stable projectile and target combinations exist. Incomplete fusion [1] or cluster transfer reactions in normal kinematics induced by stable beams [2] or inverse-kinematics reactions with radioactive projectiles and light stable targets [3–5], at low beam energies, have been used in only a very few cases to access high-spin yrast states; the latter type of studies is sparse due to the limited availability of the intense low-energy rare-isotope beams that are necessary.

Here, we extend the work on neutron-deficient nuclei reported in Ref. [6] and present the in-beam  $\gamma$ -ray spectroscopy of complex-structure, core-coupled states near the yrast line of <sup>39</sup>Ca. These states were populated in fast-beam-induced, dissipative (high-momentum-loss) reaction processes leading to single-neutron addition onto excited configurations of the projectile,  ${}^9\text{Be}({}^{38}\text{Ca}^*, {}^{39}\text{Ca} + \gamma)X$ . Complementing the analysis presented in Ref. [6], we provide further discussion on the inelastic scattering,  ${}^9\text{Be}({}^{38}\text{Ca}, {}^{38}\text{Ca} + \gamma)X$ , at high momentum loss. Figure 1 shows the location of these systems on the nuclear chart.

The neutron-deficient  $^{38}$ Ca isotope continues to attract attention due to its importance for testing fundamental symmetries [7–13] and as the compound nucleus in the  $^{34}$ Ar( $\alpha$ , p) $^{37}$ K capture reaction of relevance for x-ray bursts [14]. For nuclear structure studies,  $^{38}$ Ca can be accessed via ( $^{3}$ He, n) and (p, t) reactions from stable  $^{36}$ Ar and  $^{40}$ Ca, respectively. Hence an extensive body of work is available on, for example, pairing vibrations [15], fp-shell configurations [16], and an anomalous L=0 transition to the first excited  $0^{+}$  state. The latter was observed in the (p, t) reaction from  $^{40}$ Ca [17–20]. The intermediate-energy Coulomb excitation measurement by Cottle et al. [21], exploring isospin symmetry, is the only one using a beam of unstable  $^{38}$ Ca projectiles. The sole published studies using  $\gamma$ -ray spectroscopy are from

<sup>\*</sup>Present address: Lawrence Livermore National Laboratory, Livermore, California 94550, USA.

<sup>&</sup>lt;sup>†</sup>Present address: TRIUMF, 4004 Wesbrook Mall, Vancouver, BC V6T 2A3, Canada.

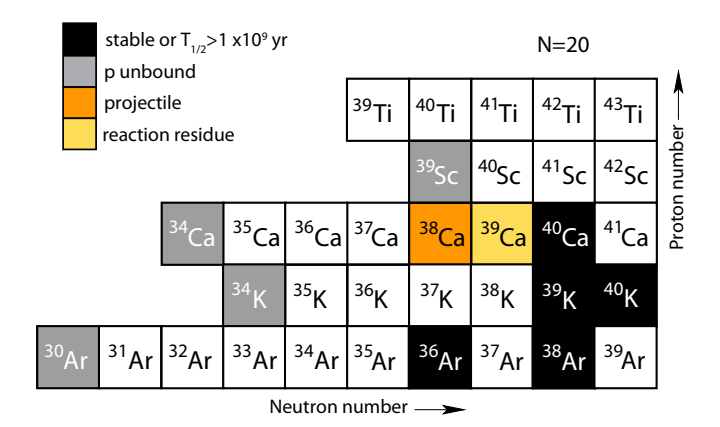


FIG. 1. Part of the nuclear chart showing the projectile beam <sup>38</sup>Ca and the one-neutron pickup residue <sup>39</sup>Ca in the proximity of the proton dripline.

1970 [22] [( $^3$ He,  $n\gamma$ ), using three Ge(Li) detectors] and 1999 [21] (intermediate-energy Coulomb excitation, using a NaI scintillator array). The National Nuclear Data Center (NNDC) further quotes  $\gamma$ -ray data from a 1974 Duke University PhD thesis [23] which appears unpublished for all practical purposes. The data presented here constitute the first  $\gamma$ -ray spectroscopy of  $^{38}$ Ca exploiting a modern, high-resolution high-purity germanium (HPGe)  $\gamma$ -ray tracking array.

Unlike for  $^{38}$ Ca, modern  $\gamma$ -ray spectroscopy data are available for  $^{39}$ Ca. For example, from (a) a recent ( $^{3}$ He,  $\alpha\gamma$ ) experiment [24], aimed at observables important for the  $^{38}$ K(p,  $\gamma$ ) $^{39}$ Ca reaction rate, and (b) from a high-spin spectroscopy study via the  $^{16}$ O( $^{28}$ Si,  $\alpha n\gamma$ ) $^{39}$ Ca reaction [25]. In the present work, we show that dissipative processes in the fast-beam one-neutron pickup channel populate the very same states as reported in the high-spin study of Ref. [25], suggesting a possible novel and practical pathway to study such states in rare isotopes. This also elucidates the observation of such states, with low yields, in the low-momentum tails of longitudinal momentum distributions in nucleon knockout experiments, reported in recent measurements.

## II. EXPERIMENT, RESULTS, AND DISCUSSION

The experimental details and setup are also discussed in Refs. [6,26] and a brief summary is provided here. The <sup>38</sup>Ca rare-isotope beam was produced at the Coupled Cyclotron Facility at NSCL [27] in the fragmentation of a stable 140-MeV/ nucleon <sup>40</sup>Ca primary beam in the A1900 fragment separator [28], on a 799 mg/cm<sup>2</sup> <sup>9</sup>Be production target and separated using a 300 mg/cm<sup>2</sup> Al degrader. The momentum width was limited to  $\Delta p/p = 0.25\%$  for optimum resolution, resulting in 160 000 <sup>38</sup>Ca /s interacting with a 188-mg/cm<sup>2</sup>-thick <sup>9</sup>Be foil placed in the center of the high-resolution y-ray tracking array GRETINA [29,30] surrounding the reaction target position of the S800 spectrograph [31]. The <sup>38</sup>Ca projectiles had a midtarget energy of 60.9 MeV/nucleon. The incoming beam and the projectile-like reaction residues were event-by-event identified using the S800 analysis beam line and focal plane [32]. The scattered <sup>38</sup>Ca and one-neutron pickup residues,

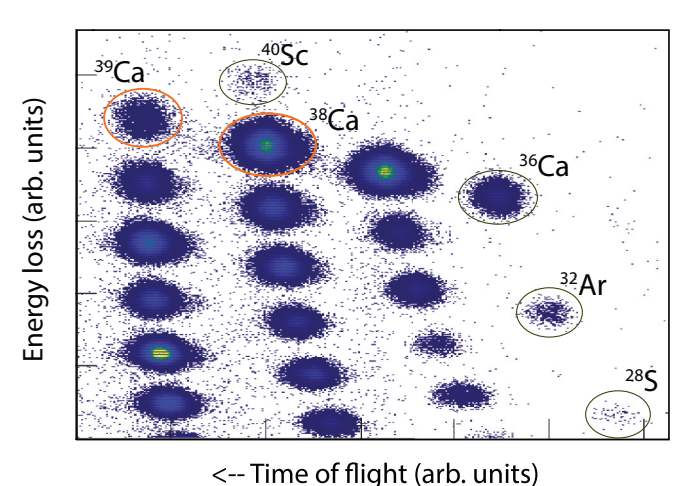


FIG. 2. Particle identification showing the same data as in Fig. 2 of Ref. [26] with <sup>38,39</sup>Ca highlighted.

<sup>39</sup>Ca, are cleanly separated in the particle identification plot displayed in Fig. 2. The magnetic rigidity of the S800 spectrograph was tuned for the two-neutron removal reaction to <sup>36</sup>Ca and so only the outermost low-momentum tails of the reacted <sup>38</sup>Ca and <sup>39</sup>Ca longitudinal momentum distributions were transmitted to the S800 focal plane, as quantified below. In the following, we will first discuss the general characteristics of the reactions and then focus on the detailed spectroscopy results for <sup>39</sup>Ca and on additional data and discussion for <sup>38</sup>Ca not presented in [6].

With the chosen magnetic rigidity, optimized for <sup>36</sup>Ca, the parts of the <sup>39</sup>Ca and <sup>38</sup>Ca momentum distributions that enter the S800 focal plane are approximately  $\pm 300~{\rm MeV}/c$ about the momentum  $p_0 = 11.222 \text{ GeV}/c$ . Figure 3 shows the measured parallel momentum distributions of (i) the lowmomentum tail of the <sup>38</sup>Ca distribution on a logarithmic scale (shown as an inset), over a slightly reduced momentum range that is not subject to further acceptance effects, and (ii) the tail of the <sup>39</sup>Ca one-neutron pickup distribution (purple curve) from the same setting. This <sup>39</sup>Ca distribution is further impacted by the focal-plane acceptance starting at about  $p_0 + 275 \text{ MeV}/c$ . The momentum distribution of the unreacted <sup>38</sup>Ca after passage through the target is also shown (blue curve, roughly centered on  $p_0 = 11.932 \text{ GeV}/c$ ) to help clarify the momentum losses in the observed <sup>39</sup>Ca and <sup>38</sup>Ca tail distributions.

The parallel momentum distribution of <sup>39</sup>Ca is cut by the S800 focal-plane acceptance on the high-momentum end, leaving only a tail within the acceptance. It is interesting to estimate where the centroid of the full distribution would be. The complication here is that this depends on the momentum of the neutron picked up from the target which is not precisely calculable, given that our reaction is highly linear-momentum mismatched and is dominated by the pickup of deeply bound, high-momentum neutrons [33]. Such fast-beam one-nucleon pickup reactions have been carried out for a number of projectiles upon <sup>12</sup>C and <sup>9</sup>Be targets within the same experimental scheme [33–37]. The only one-neutron

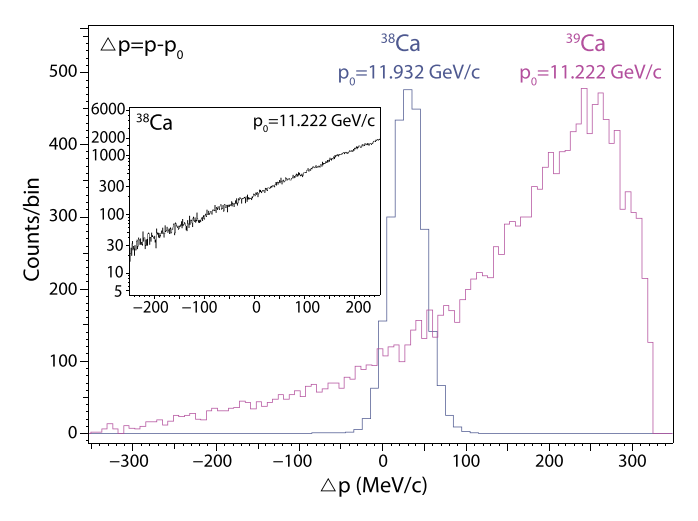


FIG. 3. Measured tails of the parallel momentum distributions, versus  $\Delta p = p - p_0$  (with  $p_0 = 11.222~{\rm GeV/c}$ ) for the <sup>39</sup>Ca one-neutron pickup residues (purple curve) and, as an inset, for the <sup>38</sup>Ca nuclei that have undergone a momentum loss of order of 700 MeV/c (black curve). The latter is shown on a logarithmic scale, revealing its exponential character. The momentum distribution versus  $\Delta p = p - p_0$  (with  $p_0 = 11.932~{\rm GeV/c}$ ) of the unreacted <sup>38</sup>Ca after passage through the target is also shown (blue curve). These central momentum values,  $p_0$ , for each isotope, correspond to the respective magnetic rigidity setting of the S800 spectrograph. The low-momentum tail distributions of the <sup>39</sup>Ca reaction residues and of the reacted <sup>38</sup>Ca entered the focal plane in the same setting and thus  $p_0$  value, while the unreacted <sup>38</sup>Ca is from a different magnetic setting with a different  $p_0$  value.

pickup from a  ${}^{9}$ Be target onto a neutron-deficient projectile was  ${}^{9}$ Be( ${}^{22}$ Mg,  ${}^{23}$ Mg + $\gamma$ )X.

So, to estimate the centroid position of the full distribution we resort to the systematics presented in Fig. 7 of Soulioutis et al. [38]. This confronts the centroid of the parallel momentum per nucleon of the pickup residues relative to the parallel momentum per nucleon of the beam, f, with the number of nucleons transferred from the target,  $\Delta A_t$ , relative to the mass of the fragment,  $A_f$ , i.e., f vs.  $\Delta A_t/A_f$ . As one would expect, the systematics show that with increasing fragment mass and a small number of nucleons transferred, f approaches 1, meaning that the parallel momentum per nucleon between the beam and pickup residues is essentially unchanged following the reaction. However, the systematics include only pickup from heavier targets, such as Al and Ta [38], and it is not a priori clear how well these may apply to the neutron pickup from the complex Be targetwhich may be viewed as having predominantly the structure of two  $\alpha$  particles plus an additional neutron. To benchmark the systematics for a one-neutron pickup from <sup>9</sup>Be onto a neutron-deficient projectile, we deduce f = 0.974 from Fig. 3 of [33] and extrapolation to a midtarget reaction vertex for  ${}^{9}\text{Be}({}^{22}\text{Mg}, {}^{23}\text{Mg} + \gamma)X$ . This result indeed fits well into the systematics of [38] at  $\Delta A_t/A_f = 0.04$ . Now, for <sup>39</sup>Ca and  $\Delta A_t/A_f = 0.026$ , an f closer to 0.990 would be expected. Using this value to calculate the parallel momentum of <sup>39</sup>Ca from pickup onto <sup>38</sup>Ca at midtarget predicts a centroid of the parallel momentum distribution, as measured behind the target, of 12.165 GeV/c, more than 600 MeV/c outside of the S800 acceptance captured by our setting. So, indeed, we appear to observe only the outermost tail of the <sup>39</sup>Ca pickup distribution. Although the fast-beam pickup reactions are very sensitive to the nuclear structure of the projectile and the beam energy, perhaps supporting that only the outermost tail is observed, the cross section determined for the part of the distribution we observe—from the number of <sup>39</sup>Ca relative to the number of <sup>38</sup>Ca projectiles and target nuclei—yields  $\sigma(p_0 \pm 330\,\text{MeV}/c) = 0.11(1)$  mb, which is more than a factor of 20 smaller than the inclusive cross section for the <sup>22</sup>Mg +n reaction reported in Ref. [33], for example.

The low-momentum tails of parallel momentum distributions in fast-beam, one-nucleon pickup, as well as in knockout reactions, have long been suspected to reveal the presence of rare, higher-order, more-dissipative processes [35,39–42]. Of particular relevance may be the observation of a core-coupled state in the  ${}^{9}\text{Be}({}^{22}\text{Mg}, {}^{23}\text{Al} + \gamma)X$  one-proton pickup reaction where a pronounced low-momentum tail dominated the measured parallel momentum distribution of <sup>23</sup>Al [35]. There, the only excited state observed was the first  $(7/2^+)$  level, almost 1400 keV above the proton separation energy, which could only be reached in a complex rearrangement: pickup of a  $d_{5/2}$  proton onto <sup>22</sup>Mg excited into the  $2_1^+$  state [35]. This was indeed supported by the fact that the excitation of the  $2_1^+$  and  $4_1^+$  states was observed in the low-momentum tail of the reacted <sup>22</sup>Mg projectiles passing through the target [35]. Our current observations display an astonishing bounty of these more-complex, higher-spin states, accessible in <sup>39</sup>Ca via in-beam  $\gamma$ -ray spectroscopy. The spectroscopy of <sup>39</sup>Ca will be discussed in the following subsection.

When compared to the parallel momentum distribution of the unreacted  $^{38}$ Ca passing through the target and suffering only in-target energy loss, the reacted  $^{38}$ Ca nuclei in the reaction setting have undergone an additional longitudinal momentum loss of about 700 MeV/c, that is 18 MeV/c per nucleon in momentum or 5.4 MeV/nucleon in energy. The logarithmic plot in the inset in Fig. 3 reveals that this low-momentum tail of the  $^{38}$ Ca parallel momentum distribution is essentially exponential. As for the pickup cross section quoted above, the cross section for finding  $^{38}$ Ca with large momentum loss in the interval  $p_0 \pm 330$  MeV/c was extracted to yield  $\sigma(p_0 \pm 330 \, \text{MeV}/c) = 3.8(4)$  mb, making these inelastic large-momentum-loss events also rather rare. See Ref. [6] for a detailed discussion of the most strongly populated configurations in  $^{38}$ Ca at high momentum loss.

## A. <sup>39</sup>Ca spectroscopy

The event-by-event Doppler reconstructed  $\gamma$ -ray spectrum measured in coincidence with the  $^{39}$ Ca reaction residues detected in the S800 focal plane is shown in Fig. 4. Nearest neighbor addback, as detailed in [30], was used. All  $\gamma$ -ray transitions observed here have been reported before, for example in Refs. [25] and [24], with unambiguous placements in the  $^{39}$ Ca level scheme. A few peculiarities of in-beam  $\gamma$ -ray spectroscopy at or above 30% of the speed of light are apparent. The v/c=0.30 chosen for the Doppler

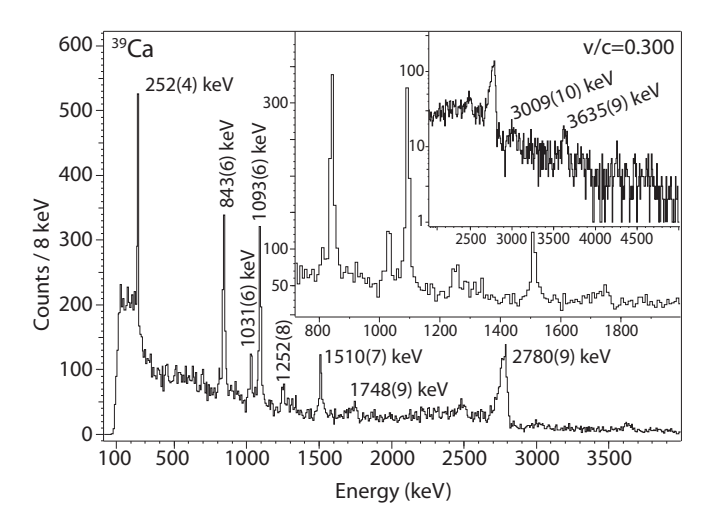


FIG. 4. Doppler-reconstructed addback  $\gamma$ -ray spectrum as detected in coincidence with the <sup>39</sup>Ca one-neutron pickup residues identified in the S800 focal plane. All  $\gamma$ -ray transitions are labeled by their energy. The two insets magnify low-statistics regions of the spectrum. All transitions are known—nine of the ten reported energies agree with the literature values within uncertainties and the discrepancy for the 2797-keV transition [25] is attributed to lifetime effects as discussed in the text.

reconstruction gives the best resolution for the presumably fast M1/E2 transitions, such as at 252, 843, 1031, and 1093 keV, while the peak quoted at 2780 keV displays a pronounced left-side tail and is too low in energy as compared to the literature value of 2796 keV [24]. This is due to the corresponding  $7/2^-$  excited-state having a long half-life of 62(17) ps [43], thus decaying well behind the target and being Doppler-reconstructed to an energy value that is too low. This effect was both discussed and simulated for this beam energy regime and setup in Ref. [44] for the case of  $^{70}$ Fe.

It is noted that there is no clear evidence for the 2467-keV  $1/2^+$  first excited state, which would also be obscured by the Compton edge of the 2780-keV  $\gamma$  ray visible at about 2500 keV. Indeed, the population of this state would not be expected in fast-beam one-neutron pickup due to the large momentum mismatch at our high beam energies. Table I provides the observed relative  $\gamma$ -ray intensities in  $^{39}$ Ca. These are

TABLE I. Relative intensities  $I_{\gamma}$  of the  $\gamma$ -ray transitions with energy  $E_{\gamma}$  extracted from the <sup>39</sup>Ca  $\gamma$ -ray spectrum shown in Fig. 4.

20(3)
41(4)
15(2)
41(4)
9(3)
18(3)
3(1)
100(10)
12(3)
15(3)

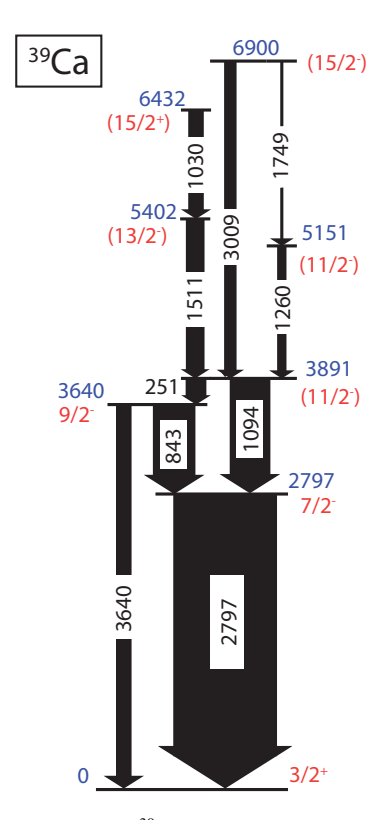


FIG. 5. Level scheme of  $^{39}$ Ca as populated in this work. The line width of the arrows corresponds to the intensities of the transitions quoted in Table I. We note that the  $^{39}$ Ca proton separation energy is  $S_p = 5.7709(6)$  MeV [45], placing the J = 15/2 states above this value. For the purpose of this level scheme, we use the energies quoted in Ref. [25], which, except for the 2797-keV transition due to lifetime effects as discussed in the text, agree within uncertainties with the present work.

obtained from the efficiency-corrected peak areas and include a 7% systematic error added in quadrature to account for uncertainties in the efficiency when including addback.

Figure 5 displays the level scheme of  $^{39}$ Ca reported from the present work where the widths of the arrows scale with the  $\gamma$ -ray intensities quoted in Table I. It is noteworthy that the level scheme populated here is essentially identical to that reported in Ref. [25] from the  $^{28}$ Si +  $^{16}$ O fusion-evaporation reaction. The only state and corresponding transition reported in Fig. 3(b) of [25] that is not observed here is a proposed (19/2<sup>-</sup>) state above 7.7 MeV in excitation energy.

These observations are in contrast to the population of final states in the  $^{40}$ Ca( $^{3}$ He,  $\alpha$ ) $^{39}$ Ca transfer reactions of Refs. [24,46]. There, a number of strong positive- and negative-parity low-spin states were reported in addition to some of the high-spin, more-complex-structure states seen here but which appear only very weakly populated in Fig. 2 of Ref. [46], for example.

From Ref. [25], relative to the 0p-0h configurations of the  $^{40}$ Ca ground state, the configurations of the states observed in the  $^{39}$ Ca level scheme are dominated by (i) 0p-1h for the  $3/2^+$  ground state, (ii) 1p-2h for the  $7/2^-$  to  $13/2^-$  negative-parity multiplet, (iii) 2p-3h for the  $15/2^+$  state (one of the lowest-lying members of the stretched  $\pi(f_{7/2}) \otimes$ 

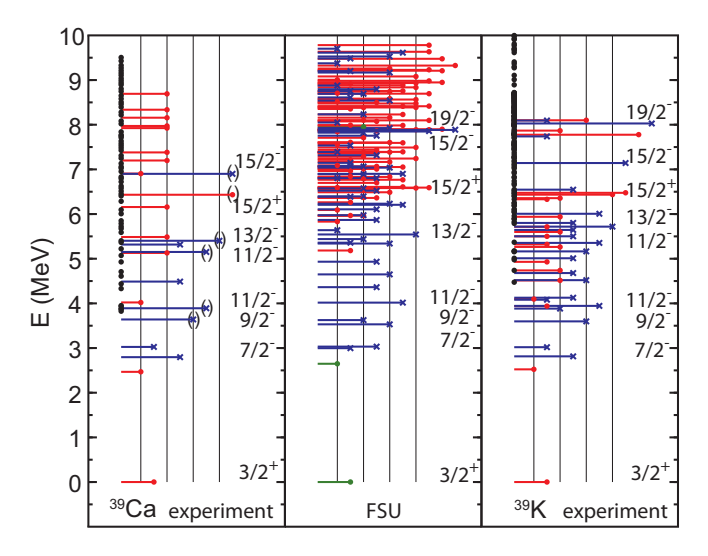


FIG. 6. Comparison of the energies of the low-lying states of  $^{39}$ Ca, with the states observed here labeled, with shell-model calculations using the FSU spsdfp interaction and the mirror nucleus  $^{39}$ K [43]. In these plots, the length of the levels indicates the J value and the color positive parity (red), negative parity (blue), and sd-shell origin (green). For the panels showing experimental data, the black dots indicate levels with unknown spin-parity assignment.

 $v(f_{7/2})$  7<sup>+</sup> configuration coupled to the K=1/2 component of the  $d_{3/2}^{-3}$  configuration), and (iv) 3p-4h for the 15/2<sup>-</sup> state which is calculated to be one of the lowest-lying members of the resulting multiplet. The present calculations for 3p-4h are limited to the 15/2<sup>-</sup> and 19/2<sup>-</sup> states shown in Fig. 6.

One might be tempted to consider complex two-step production mechanisms on different target nuclei, such as proton removal from  $^{38}$ Ca with subsequent pn pickup, but estimates are that these would have a combined cross section orders of magnitude too small—the pn pickup cross section was determined to be of order  $\mu b$ , as reported in [26]. In the absence of more exclusive data to elucidate the reaction mechanisms, it appears reasonable to speculate that the population of the observed states involves one-neutron pickup onto a  $^{38}$ Ca core that has undergone single or multiple nucleon rearrangements relative to the ground-state configuration.

While the above-mentioned dominant shell-model configurations originate from the calculations of Ref. [25]—in the very truncated  $d_{3/2} - f_{7/2}$  model space but allowing for all configurations of seven valence particles—it is interesting to compare the data also to new calculations in an extended model space (spsdf p) using a modern cross-shell interaction (FSU) [47,48] restricted to pure  $\hbar\omega$  configurations. The comparison is shown in Fig. 6 and shows a remarkable agreement between the measured <sup>39</sup>Ca energies and the calculations and highlights the mirror symmetry between Ca and K at A = 39. In the A = 39 mirror system, the second  $11/2^-$  state near 5 MeV and first 15/2<sup>-</sup> state near 7 MeV are about 1 MeV lower in energy than that calculated. The close spacing of the  $15/2^-$  and  $19/2^-$  in the calculation is a reflection of the close spacing predicted and observed for the  $(fp)^3$  configuration in <sup>43</sup>Sc and <sup>43</sup>Ti. The more rotational like spacing of the experimental  $11/2^-$ ,  $15/2^-$ , and  $19/2^-$  energies in  $^{\bar{3}9}$ K may

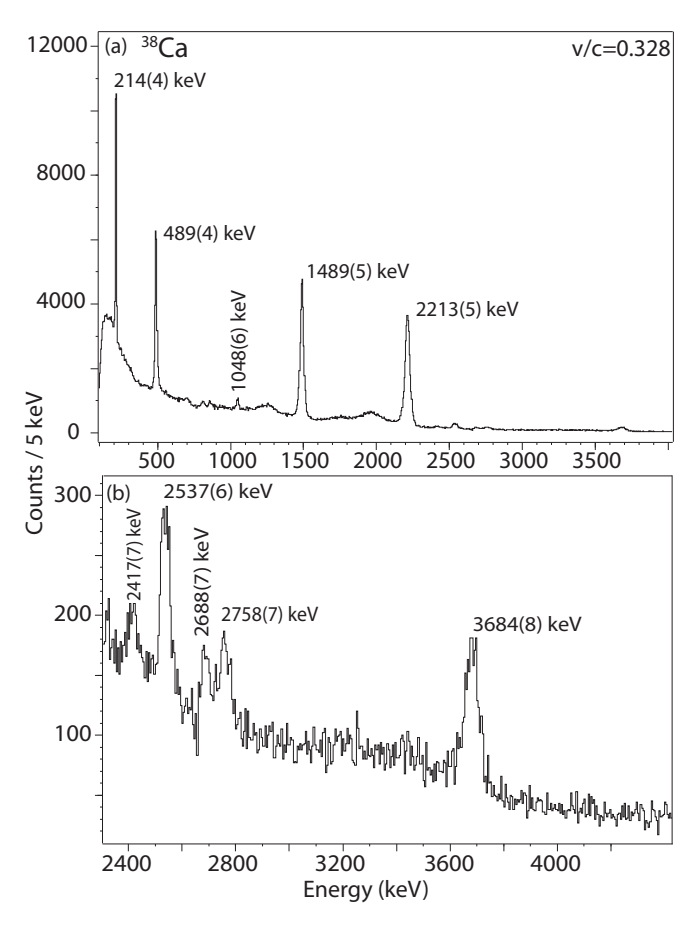


FIG. 7. Doppler-reconstructed addback  $\gamma$ -ray spectrum as detected in coincidence with the scattered  $^{38}$ Ca nuclei that underwent a large momentum loss. All  $\gamma$ -ray transitions are labeled by their energy. Panels (a) and (b) show the low-energy and high-energy region of the spectrum, respectively.

be due to deformation beyond that contained in the 3p-4h truncation.

## B. <sup>38</sup>Ca spectroscopy

Complementing the spectroscopy data and shell-model theory discussion published in Ref. [6], presented here is the full level scheme including very weak transitions and the corresponding coincidence relationships not discussed in [6], all relative peak intensities with their uncertainties, and the determination of an upper limit for the  $3_1^- \rightarrow 0_1^+$  branch which is relevant for Coulomb excitation studies that report population of the near-degenerate  $3_1^-$  and  $2_2^+$  states.

The event-by-event Doppler reconstructed  $\gamma$ -ray spectrum obtained in coincidence with the <sup>38</sup>Ca reaction residues detected in the S800 focal plane at large momentum loss is shown in Fig. 7. Nearest neighbor addback, as detailed in [30], was used. Of the seven  $\gamma$ -ray transitions compiled in [23], those at 2213(5), 1489(5), 489(4), 3684(8) keV are observed here, while the transitions at 214(4), 1048(6), 2417(7), 2537(6), 2688(7), and 2758(7) keV are reported for the first time in the present work (see also [6]).

TABLE II. Relative intensities  $I_{\gamma}$  of the  $\gamma$ -ray transitions with energy  $E_{\gamma}$  extracted from the <sup>38</sup>Ca  $\gamma$ -ray spectrum shown in Fig. 7.

$E_{\gamma}$ (keV)	$I_{\gamma}$ (%)
214(4)	27(2)
489(4)	31(2)
1048(6)	3.0(5)
1489(5)	75(5)
2213(5)	100(7)
2417(7)	1.8(3)
2537(6)	4.8(5)
2688(7)	2.0(3)
2758(7)	2.9(4)
3684(8)	6.6(6)

Table II lists the relative  $\gamma$ -ray intensities deduced from the efficiency-corrected peak areas from the spectrum displayed in Fig. 7. These include a 7% error, added in quadrature, to account for the uncertainty in the photopeak efficiency with addback. Remarkably, the fourth strongest  $\gamma$  ray, at 214 keV, has not been reported previously.

To construct the level scheme,  $\gamma \gamma$  coincidences were used. The level scheme, comprising the transitions with 3% or more relative intensity in the above table, is discussed in detail in Ref. [6]. For placement of the weaker transitions not previously discussed, Fig. 8 shows the coincidence analysis of the higher-energy part of the <sup>38</sup>Ca spectrum (right) in addition to the clear coincidences present below 2.5 MeV (left). On the right, the figure shows the high-energy part of the projection of the  $\gamma\gamma$  coincidence matrix and cuts on the three strongest  $\gamma$ -ray transitions in this energy region. There is evidence that the four  $\gamma$  rays between 2417 and 2758 keV are in coincidence with 2213 keV and that the 2417-keV transition is coincident to 489 keV. We note that there was no evidence for any of the high-energy  $\gamma$  rays in the coincidence spectrum with 214 keV which is not shown here. The narrow feature at 2268 keV in the spectrum coincident to 1489 keV is not visible in the singles spectrum and is not claimed as a transition here. Curiously, the 3684-keV transition, present in the projection of the coincidence matrix, appears coincident with  $\gamma$  rays between 4 and 6.5 MeV, as shown in the inset.

Figure 9 shows the resulting level scheme with the intensities of the  $\gamma$ -ray transitions indicated by the line width of the arrows.

The 2688 and 2758-keV transitions, which appear to feed the  $2_1^+$  state, establish levels at 4901 and 4972 keV, respectively. The first of these two levels likely corresponds to the previously reported  $2^+$  at 4902 keV [23], while the 4971-keV state might be the mirror level of the  $^{38}$ Ar ( $^{2}$ ) state at 5084 keV [23] which decays predominantly to the first  $2^+$  state, as observed here. The 2417-keV transition on top of the ( $^{4}$ ) state suggests a level at 6608 keV in  $^{38}$ Ca. The only level in the mirror nucleus in that energy region, that decays the strongest to the  $^{4}$  state, is another  $^{4}$  level at 6602 keV [23]. It is, however, peculiar that the mirror level in  $^{38}$ Ar would now

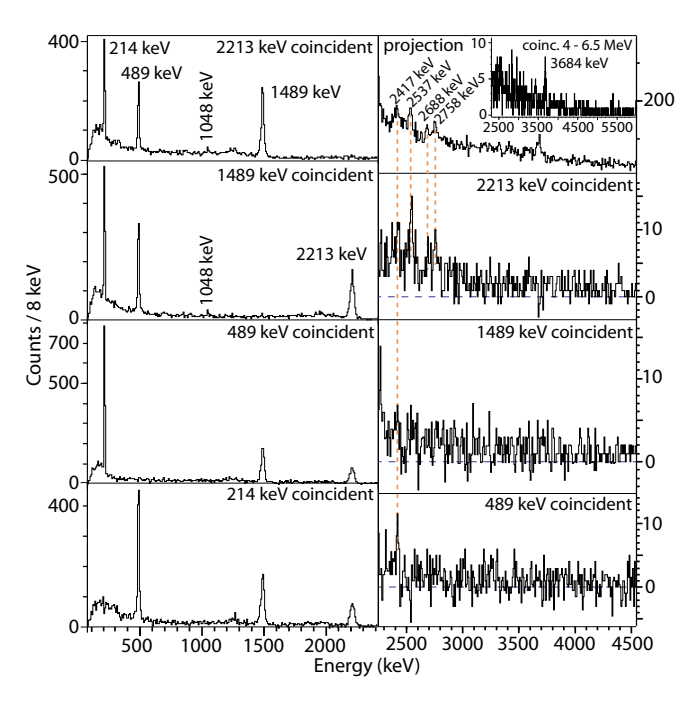


FIG. 8. Left: Coincidence relationships in the lower-energy part of the spectrum, with a clear level scheme emerging from these (see Fig. 9 and [6]). Right: Doppler-corrected projection of the  $\gamma\gamma$  matrix in the higher-energy region of the spectrum and coincidence spectra in this energy range obtained from cuts on the labeled transitions. Background was subtracted via a cut of equal width at slightly higher energy. Evidence for coincidence relationships is present also in the higher-energy region of the spectra. The inset shows that there may be unresolved weak high-energy transitions that feed the 3684-keV state.

be about equal in energy, while they are significantly higher for the other negative-parity states [23].

The present data can also shed further light on the Coulomb excitation work of Ref. [21] where two states were proposed to be excited (see Fig. 1 of [21]), with two transitions depopulating the 3685-keV 2<sub>2</sub><sup>+</sup> level. The picture emerging here is rather that, in fact, three states may be excited: the first 2<sup>+</sup>, the second  $2^+$ , and the first  $3^-$  states. The 1479-, 2206-, and 3685keV transitions reported in [21] would then correspond to the  $(3_1^-) \rightarrow 2_1^+, 2_1^+ \rightarrow 0_1^+$ , and  $2_2^+ \rightarrow 0_1^+$  decays, respectively. While we cannot exclude the existence of a weak  $2^+_2 \rightarrow 2^+_1$ transition, due to the proximity to the spectrum-dominating 1489-keV  $\gamma$  ray, as discussed above, we can limit the  $(3_1^-) \rightarrow$  $0_1^+$  transition that was briefly discussed in [21]. Figure 10 shows a coincidence spectrum obtained by gating on the 489keV transition that feeds predominantly the  $(3_1^-)$  state. Given the photopeak efficiencies and assuming that there are at most three counts at 3702 keV, we can limit the branching ratio for the  $(3^-)$  decay to the ground state to  $\leq 1\%$ .

Similar to the case of <sup>39</sup>Ca, discussed above, the configurations of the states populated in the dissipative scattering discussed here appear to require the simultaneous rearrangement of several nucleons in a single collision, giving hitherto unconsidered access to complex-structure states in rare isotopes [6].

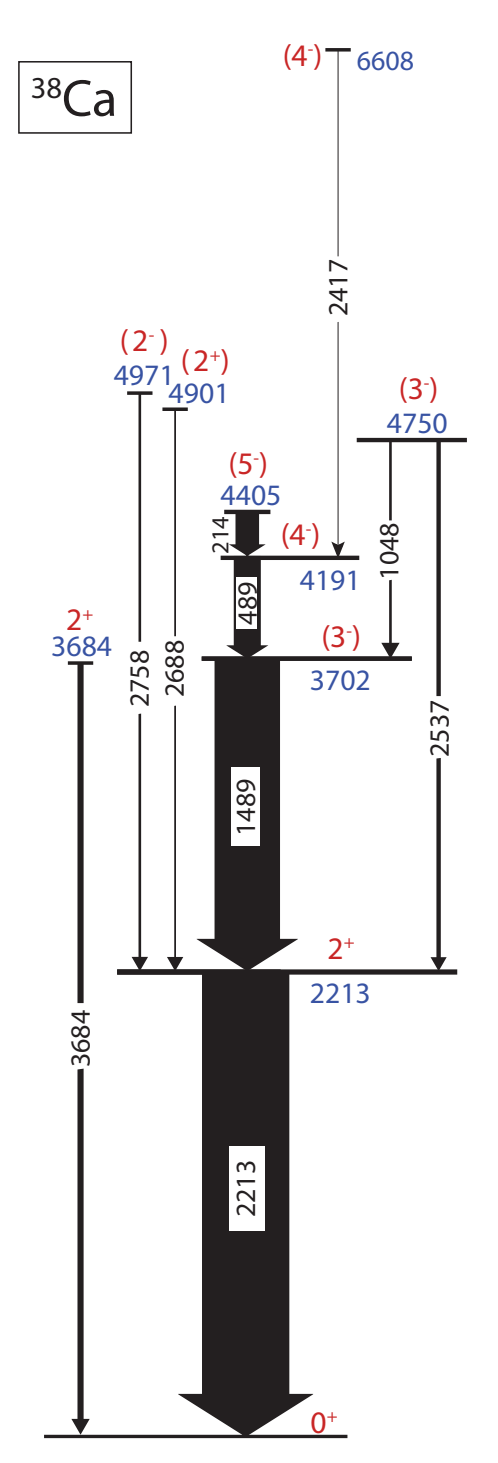


FIG. 9. Proposed level scheme for  $^{38}$ Ca, extended version based on Ref. [6]. The width of the arrows is proportional to the  $\gamma$ -ray intensity of the corresponding transition. The proton separation energy of  $S_p = 4.54727(22)$  MeV [45] places the four highest-excited states in this level scheme above the proton separation energy. Spin-parity assignments in parenthesis are tentative.

#### III. SUMMARY

In this work, the population of higher-spin complex-structure states at high momentum loss, discussed in Ref. [6] for <sup>38</sup>Ca excited following inelastic scattering off <sup>9</sup>Be, is

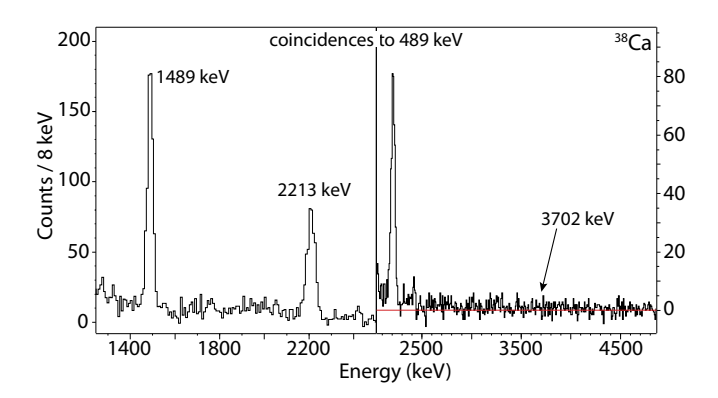


FIG. 10. Coincidence spectrum gated on the 489-keV feeder to the  $(3_1^-)$  level at 3702 keV. No evidence for the  $(3_1^-) \rightarrow 0_1^+$  transition at 3702 keV is observed.

extended to the case of fast-beam-induced single-neutron pickup onto excited-state configurations of the projectile,  $^{9}$ Be( $^{38}$ Ca\*,  $^{39}$ Ca+ $\gamma$ )X. The states populated in the lowmomentum tail of the <sup>39</sup>Ca one-neutron pickup parallel momentum distribution, with total angular momenta up to J = 15/2, are the same as observed in high-spin spectroscopy following a fusion-evaporation reaction. There is no evidence for population of the low-spin states usually reported in the <sup>40</sup>Ca-induced light-ion nucleon transfer reactions. As proposed in Ref. [6] for <sup>38</sup>Ca, the excited states of <sup>39</sup>Ca formed in one-neutron pickup onto <sup>38</sup>Ca at high momentum loss are consistent with the simultaneous rearrangement of multiple nucleons in a single energetic collision with a <sup>9</sup>Be target nucleus. It is argued that the same mechanism is responsible for the weak population of complex-structure states often reported in the low-momentum tails of one-nucleon knockout longitudinal momentum distributions. Complementing the discussion of <sup>38</sup>Ca in Ref. [6], the complete spectroscopy data on this nucleus from the present work is provided. While the detailed mechanism(s) responsible for the largemomentum-loss events observed in the reactions remain unexplained at present, these pose an interesting experimental challenge. Their clarification would certainly require a characterization of the target breakup channels. Regardless of the detailed reaction mechanism(s), this work demonstrates that exploiting such dissipative processes offers the potential to use high-luminosity, fast-beam-induced reactions to perform higher-spin spectroscopy of rare isotopes.

#### ACKNOWLEDGMENTS

This work was supported by the U.S. National Science Foundation (NSF) under Grants No. PHY-1565546 and no. PHY-2110365, by the DOE National Nuclear Security Administration through the Nuclear Science and Security Consortium, under Award No. DE-NA0003180, and by the U.S. Department of Energy, Office of Science, Office of Nuclear Physics, under Grants No. DE-SC0020451 (MSU) and No. DE-FG02-87ER-40316 (WashU), and under Contract No. DE-AC02-06CH11357 (ANL). GRETINA was funded by the

DOE, Office of Science. Operation of the array at NSCL was supported by the DOE under Grant No. DE-SC0019034.

- J.A.T. acknowledges support from the Science and Technology Facilities Council (U.K.) Grant No. ST/V001108/1.
- [1] G. D. Dracoulis, A. P. Byrne, T. Kibedi, T. R. McGoram, and S. M. Mullins, J. Phys. G: Nucl. Part. Phys. 23, 1191 (1997).
- [2] D. R. Haenni, T. T. Sugihara, R. P. Schmitt, G. Mouchaty, and U. Garg, Phys. Rev. C 25, 1699 (1982).
- [3] E. Ideguchi, M. Niikura, C. Ishida, T. Fukuchi, H. Baba, N. Hokoiwa, H. Iwasaki, T. Koike, T. Komatsubara, T. Kubo, M. Kurokawa, S. Michimasa, K. Miyakawa, K. Morimoto, T. Ohnishi, S. Ota, A. Ozawa, S. Shimoura, T. Suda, M. Tamaki, I. Tanihata, Y. Wakabayashi, K. Yoshida, and B. Cederwall, Eur. Phys. J. A 25, 429 (2005).
- [4] S. Bottoni, S. Leoni, B. Fornal, R. Raabe, K. Rusek, G. Benzoni et al., Phys. Rev. C 92, 024322 (2015).
- [5] J. Ash, H. Iwasaki, T. Mijatovic, T. Budner, R. Elder, B. Elman, M. Friedman, A. Gade, M. Grinder, J. Henderson, B. Longfellow, A. Revel, D. Rhodes, M. Spieker, Y. Utsuno, D. Weisshaar, and C. Y. Wu, Phys. Rev. C 103, L051302 (2021).
- [6] A. Gade, B. A. Brown, D. Weisshaar, D. Bazin, K. W. Brown, R. J. Charity, P. Farris, A. M. Hill, J. Li, B. Longfellow, D. Rhodes, W. Reviol, and J. A. Tostevin, Phys. Rev. Lett. 129, 242501 (2022).
- [7] G. Bollen, D. Davies, M. Facina, J. Huikari, E. Kwan, P. A. Lofy, D. J. Morrissey, A. Prinke, R. Ringle, J. Savory, P. Schury, S. Schwarz, C. Sumithrarachchi, T. Sun, and L. Weissman, Phys. Rev. Lett. 96, 152501 (2006).
- [8] R. Ringle, T. Sun, G. Bollen, D. Davies, M. Facina, J. Huikari, E. Kwan, D. J. Morrissey, A. Prinke, J. Savory, P. Schury, S. Schwarz, and C. S. Sumithrarachchi, Phys. Rev. C 75, 055503 (2007).
- [9] S. George, S. Baruah, B. Blank, K. Blaum, M. Breitenfeldt, U. Hager, F. Herfurth, A. Herlert, A. Kellerbauer, H.-J. Kluge, M. Kretzschmar, D. Lunney, R. Savreux, S. Schwarz, L. Schweikhard, and C. Yazidjian, Phys. Rev. Lett. 98, 162501 (2007).
- [10] H. I. Park, J. C. Hardy, V. E. Iacob, A. Banu, L. Chen, V. V. Golovko, J. Goodwin, V. Horvat, N. Nica, E. Simmons, L. Trache, and R. E. Tribble, Phys. Rev. C 84, 065502 (2011).
- [11] H. I. Park, J. C. Hardy, V. E. Iacob, M. Bencomo, L. Chen, V. Horvat, N. Nica, B. T. Roeder, E. Simmons, R. E. Tribble, and I. S. Towner, Phys. Rev. Lett. 112, 102502 (2014).
- [12] H. I. Park, J. C. Hardy, V. E. Iacob, M. Bencomo, L. Chen, V. Horvat, N. Nica, B. T. Roeder, E. McCleskey, R. E. Tribble, and I. S. Towner, Phys. Rev. C 92, 015502 (2015).
- [13] B. Blank, J.-C. Thomas, P. Ascher, L. Audirac, A. Bacquias, L. Caceres, G. Canchel, L. Daudin, F. de Oliveira Santos, F. Didierjean, M. Gerbaux, J. Giovinazzo, S. Grevy, T. Kurtukian Nieto, I. Matea, F. Munoz, M. Roche, L. Serani, N. Smirnova, and J. Souin, Eur. Phys. J. A 51, 8 (2015).
- [14] A. M. Long, T. Adachi, M. Beard, G. P. A. Berg, Z. Buthelezi, J. Carter, M. Couder, R. J. deBoer, R. W. Fearick, S. V. Fortsch, J. Gorres, J. P. Mira, S. H. T. Murray, R. Neveling, P. Papka, F. D. Smit, E. Sideras-Haddad, J. A. Swartz, R. Talwar, I. T. Usman, M. Wiescher et al., Phys. Rev. C 95, 055803 (2017).
- [15] W. Bohne, K. D. Buchs, H. Fuchs, K. Grabisch, D. Hilscher, U. Jahnke, H. Kluge, T. G. Masterson, and H. Morgenstern, Nucl. Phys. A 284, 14 (1977).

- [16] W. P. Alford, P. Craig, D. A. Lind, R. S. Raymond, J. Ullman, C. D. Zafiratos, and B. H. Wildenthal, Nucl. Phys. A 457, 317 (1986).
- [17] J. C. Hardy, D. J. Skyrme, and I. S. Towner, Phys. Lett. 23, 487 (1966).
- [18] S. Kubono, S. Kato, M. Yasue, H. Ohnuma, and K. Ogawa, Phys. Lett. B 49, 37 (1974).
- [19] S. Kubono, S. Kato, M. Yasue, H. Ohnuma, M. Sasao, K. Tsukamoto, and R. Kuramasu, Nucl. Phys. A 276, 201 (1977).
- [20] R. A. Paddock, Phys. Rev. C 5, 485 (1972).
- [21] P. D. Cottle, M. Fauerbach, T. Glasmacher, R. W. Ibbotson, K. W. Kemper, B. Pritychenko, H. Scheit, and M. Steiner, Phys. Rev. C 60, 031301(R) (1999).
- [22] M. H. Shapiro, A. Adams, C. Moss, and W. M. Denny, Nucl. Phys. A 144, 17 (1970).
- [23] J. Chen, Nucl. Data Sheets 152, 1 (2018).
- [24] M. R. Hall, D. W. Bardayan, T. Baugher, A. Lepailleur, S. D. Pain, A. Ratkiewicz, S. Ahn, J. M. Allen, J. T. Anderson, A. D. Ayangeakaa, J. C. Blackmon, S. Burcher, M. P. Carpenter, S. M. Cha, K. Y. Chae, K. A. Chipps, J. A. Cizewski, M. Febbraro, O. Hall, J. Hu et al., Phys. Rev. C 101, 015804 (2020).
- [25] Th. Andersson, D. Rudolph, C. Baktash, J. Eberth, C. Fahlander, D. Haslip, D. R. LaFosse, S. D. Paul, D. G. Sarantites, C. E. Svensson, H. G. Thomas, J. C. Waddington, W. Weintraub, J. N. Wilson, and B. A. Brown, Eur. Phys. J. A 6, 5 (1999).
- [26] A. Gade, D. Weisshaar, B. A. Brown, J. A. Tostevin, D. Bazin, K. Brown, R. J. Charity, P. J. Farris, A. M. Hill, J. Li, B. Longfellow, W. Reviol, and D. Rhodes, Phys. Lett. B 808, 135637 (2020).
- [27] A. Gade and B. M. Sherrill, Phys. Scr. 91, 053003 (2016).
- [28] D. J. Morrissey, B. M. Sherrill, M. Steiner, A. Stolz, and I. Wiedenhöver, Nucl. Instrum. Methods Phys. Res. B 204, 90 (2003).
- [29] S. Paschalis *et al.*, Nucl. Instrum. Methods Phys. Res. A 709, 44 (2013).
- [30] D. Weisshaar, D. Bazin, P. C. Bender, C. M. Campbell, F. Recchia, V. Bader, T. Baugher, J. Belarge, M. P. Carpenter, H. L. Crawford, M. Cromaz, B. Elman, P. Fallon, A. Forney, A. Gade, J. Harker, N. Kobayashi, C. Langer, T. Lauritsen, I. Y. Lee *et al.*, Nucl. Instrum. Methods Phys. Res. A **847**, 187 (2017).
- [31] D. Bazin, J. A. Caggiano, B. M. Sherrill, J. Yurkon, and A. Zeller, Nucl. Instrum. Methods Phys. Res. B 204, 629 (2003).
- [32] J. Yurkon, D. Bazin, W. Benenson, D. J. Morrissey, B. M. Sherrill, D. Swan, and R. Swanson, Nucl. Instrum. Methods Phys. Res. A 422, 291 (1999).
- [33] A. Gade, J. A. Tostevin, T. Baugher, D. Bazin, B. A. Brown, C. M. Campbell, T. Glasmacher, G. F. Grinyer, S. McDaniel, K. Meierbachtol, A. Ratkiewicz, S. R. Stroberg, K. A. Walsh, D. Weisshaar, and R. Winkler, Phys. Rev. C 83, 054324 (2011).
- [34] A. Gade, P. Adrich, D. Bazin, M. D. Bowen, B. A. Brown, C. M. Campbell, J. M. Cook, T. Glasmacher, K. Hosier, S.

- McDaniel, D. McGlinchery, A. Obertelli, L. A. Riley, K. Siwek, J. A. Tostevin, and D. Weisshaar, Phys. Rev. C 76, 061302(R) (2007).
- [35] A. Gade, P. Adrich, D. Bazin, M. D. Bowen, B. A. Brown, C. M. Campbell, J. M. Cook, T. Glasmacher, K. Hosier, S. McDaniel, D. McGlinchery, A. Obertelli, L. A. Riley, K. Siwek, J. A. Tostevin, and D. Weisshaar, Phys. Lett. B 666, 218 (2008).
- [36] S. McDaniel, A. Gade, J. A. Tostevin, T. Baugher, D. Bazin, B. A. Brown, J. M. Cook, T. Glasmacher, G. F. Grinyer, A. Ratkiewicz, and D. Weisshaar, Phys. Rev. C 85, 014610 (2012).
- [37] A. Gade, J. A. Tostevin, V. Bader, T. Baugher, D. Bazin, J. S. Berryman, B. A. Brown, D. J. Hartley, E. Lunderberg, F. Recchia, S. R. Stroberg, Y. Utsuno, D. Weisshaar, and K. Wimmer, Phys. Rev. C 93, 031601(R) (2016).
- [38] G. A. Souliotis, D. J. Morrissey, N. A. Orr, B. M. Sherrill, and J. A. Winger, Phys. Rev. C 46, 1383 (1992).
- [39] S. R. Stroberg, A. Gade, J. A. Tostevin, V. M. Bader, T. Baugher, D. Bazin, J. S. Berryman, B. A. Brown, C. M. Campbell, K. W. Kemper, C. Langer, E. Lunderberg, A. Lemasson, S. Noji, F. Recchia, C. Walz, D. Weisshaar, and S. J. Williams, Phys. Rev. C 90, 034301 (2014).
- [40] A. Mutschler, O. Sorlin, A. Lemasson, D. Bazin, C. Borcea, R. Borcea, A. Gade, H. Iwasaki, E. Khan, A. Lepailleur, F. Recchia, T. Roger, F. Rotaru, M. Stanoiu, S. R. Stroberg, J. A. Tostevin, M. Vandebrouck, D. Weisshaar, and K. Wimmer, Phys. Rev. C 93, 034333 (2016).

- [41] H. L. Crawford, A. O. Macchiavelli, P. Fallon, M. Albers, V. M. Bader, D. Bazin, C. M. Campbell, R. M. Clark, M. Cromaz, J. Dilling, A. Gade, A. Gallant, J. D. Holt, R. V. F. Janssens, R. Krücken, C. Langer, T. Lauritsen, I. Y. Lee, J. Menendez, S. Noji et al., Phys. Rev. C 95, 064317 (2017).
- [42] M. Spieker, A. Gade, D. Weisshaar, B. A. Brown, J. A. Tostevin, B. Longfellow, P. Adrich, D. Bazin, M. A. Bentley, J. R. Brown, C. M. Campbell, C. Aa. Diget, B. Elman, T. Glasmacher, M. Hill, B. Pritychenko, A. Ratkiewicz, and D. Rhodes, Phys. Rev. C 99, 051304(R) (2019).
- [43] J. Chen, Nucl. Data Sheets 149, 1 (2018).
- [44] A. Gade, R. V. F. Janssens, J. A. Tostevin, D. Bazin, J. Belarge, P. C. Bender, S. Bottoni, M. P. Carpenter, B. Elman, S. J. Freeman, T. Lauritsen, S. M. Lenzi, B. Longfellow, E. Lunderberg, A. Poves, L. A. Riley, D. K. Sharp, D. Weisshaar, and S. Zhu, Phys. Rev. C 99, 011301(R) (2019).
- [45] M. Wang, W. J. Huang, F. G. Kondev, G. Audi, and S. Naimi, Chin. Phys. C 45, 030003 (2021).
- [46] K. Setoodehnia, C. Marshall, J. H. Kelley, J. Liang, F. Portillo Chaves, and R. Longland, Phys. Rev. C 98, 055804 (2018).
- [47] R. S. Lubna, K. Kravvaris, S. L. Tabor, Vandana Tripathi, A. Volya, E. Rubino, J. M. Allmond, B. Abromeit, L. T. Baby, and T. C. Hensley, Phys. Rev. C 100, 034308 (2019).
- [48] R. S. Lubna, K. Kravvaris, S. L. Tabor, Vandana Tripathi, E. Rubino, and A. Volya, Phys. Rev. Res. 2, 043342 (2020).